The Astrophysical Journal, 750:55 (5pp), 2012 May 1 doi:10.1088/0004-637X/750/1/55

THE ROLES OF RADIATION AND RAM PRESSURE IN DRIVING GALACTIC WINDS

Mahavir Sharma and Biman B. Nath
Raman Research Institute, Sadashiva Nagar, Bangalore 560 080, India; mahavir@rri.res.in, biman@rri.res.in
Received 2011 November 3; accepted 2012 February 27; published 2012 April 13

ABSTRACT

We study gaseous outflows from disk galaxies driven by the combined effects of ram pressure on cold gas clouds and radiation pressure on dust grains. Taking into account the gravity due to disk, bulge, and dark matter halo, and assuming continuous star formation in the disk, we show that radiation or ram pressure alone is not sufficient to drive escaping winds from disk galaxies and that both processes contribute. We show that in the parameter space of star formation rate (SFR) and rotation speed of galaxies the wind speed in galaxies with rotation speeds $v_c \leqslant 200$ km s^{-1} and SFR $\leqslant 100\,M_\odot$ yr^{-1} has a larger contribution from ram pressure, and that in high-mass galaxies with large SFR radiation from the disk has a greater role in driving galactic winds. The ratio of wind speed to circular speed can be approximated as $v_w/v_c \sim 10^{0.7}\,[\mathrm{SFR}/50\,\mathrm{M}_\odot\,\mathrm{yr}^{-1}]^{0.4}\,[v_c/120\,\mathrm{km\,s}^{-1}]^{-1.25}$. We show that this conclusion is borne out by observations of galactic winds at low and high redshift and also of circumgalactic gas. We also estimate the mass loading factors under the combined effect of ram and radiation pressure, and show that the ratio of mass-loss rate to SFR scales roughly as $v_c^{-1}\Sigma_g^{-1}$, where Σ_g is the gas column density in the disk.

Key words: galaxies: evolution – galaxies: starburst – intergalactic medium

Online-only material: color figure

1. INTRODUCTION

Galactic winds have been observed at different wavelengths in galaxies of various masses and in a range of redshifts. Galaxies, especially those with star formation rate surface density (Σ_{SFR}) $\geqslant 10^{-1}\,M_\odot$ yr^{-1} kpc^{-2}, often show large outflow of hot gas that emits X-rays and in which cold clouds are found to be embedded, which are observed with Hα or NaD lines (Heckman et al. 2000; Martin 2005). The speed of the clouds in the wind range from a few tens to several hundred km s^{-1}, and the total mass-loss rate can be several times the SFR (Veilleux et al. 2005).

These outflows play a crucial role in the evolution of galaxies by expunging gas and thereby suppressing the star formation. The attempts to understand galactic evolution in the cosmological context have since long encountered the so-called cooling catastrophe problem, since left to its own device the baryonic gas would cool and form stars more rapidly than observed. It is generally believed that a feedback loop inhibits this, and that the process of star formation excites an outflow and quenches itself. The observed mass–metallicity relation in galaxies also indicates that galactic outflows play a major role in the chemical evolution in galaxies. Furthermore, these outflows enrich the intergalactic medium with metals (Nath & Trentham 1997; Ferrara et al. 2000; Madau et al. 2001).

The standard model to understand galactic outflows involves a heated interstellar medium under the influence of supernovae (SNe), and the hot gas being driven by thermal pressure (Chevalier & Clegg 1985; Heckman 2002). The expansion speed of this hot gas can be large enough to eject it out of the galaxy (Larson 1974; Saito 1979; Dekel & Silk 1986). The observations of cold gas in these outflows (Heckman et al. 2000) led to the proposal that the cold gas entrained in the hot gas moved due to ram pressure. The wind speed was, however, not found to correlate with galaxy mass (Heckman et al. 2000; Martin 1999), and it was argued that the SN rate increased with SFR and hence the wind velocity might correlate with SFR. Simulations also supported this scenario (Suchkov et al. 1994; Strickland & Stevens 2000). However, there is a limiting cloud speed implicit in this process since ram pressure acts on the cold gas until the cold gas velocity becomes equal to that of hot gas.

This scenario, however, has met with problems from new observations of cold component which show that the terminal outflow speed depends on galactic properties like rotation speed (Martin 2005; Rupke et al. 2005). It has been proposed that these observations can be explained by radiation pressure driving the outflow (Murray et al. 2005; Martin 2005; Sharma et al. 2011). It has also been pointed out that a natural course of events leading from a starburst would be a radiation pressure driven wind in the beginning, and ram pressure acting on it after a period of ∼3–5 Myr, the lifetime of massive stars (Nath & Silk 2009; Murray et al. 2011). This scenario also naturally explains the puzzling fact that cold clouds are observed at large distances although their survival timescales in the hot gas would have inhibited them from being pushed out to such distances.

In the face of two processes leading to outflows, one wonders if both processes contribute equally, or if there are regimes in which one of these two processes dominate over the other. In this paper, we present an analytical calculation for the dynamics of cold clouds taking into account both ram and radiation pressure and all sources of gravity, and compare our results with observations.

2. GASEOUS OUTFLOWS WITH RAM AND RADIATION PRESSURE

We consider the dynamics of cold clouds ($T \lesssim 10^4$ K) embedded in hot gas, in which the hot gas component exerts a drag force due to ram pressure. We also assume that dust grains in the cold clouds are strongly coupled to the gas, and therefore the dynamics of these clouds is also influenced by radiation pressure. We ignore magnetic forces and the compression of cold clouds by hot wind gas.

We therefore solve the following equation for the momentum of the cold cloud ($P_c = M_c v$), see Figure 1:

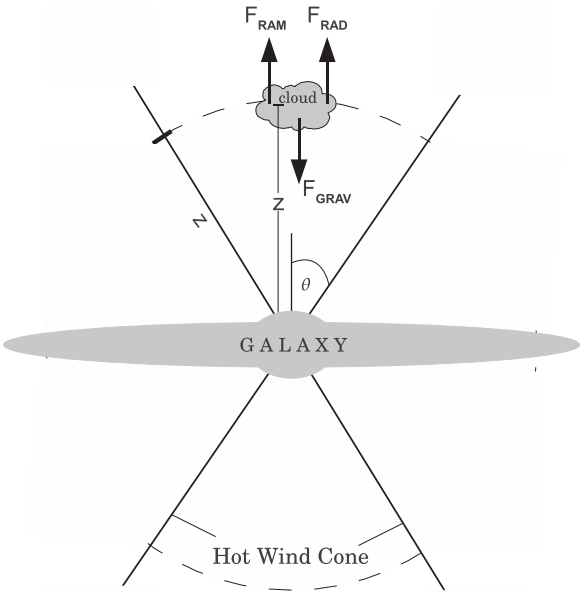

Figure 1. Schematic diagram for the motion of a cold cloud embedded in a cone of hot flow and acted upon by forces of radiation and gravity from the parent galaxy. Cloud is at a height z. The total mass loss in hot flow, $\dot{M}_h = 2\,\rho_h v_h A$, where A is the area at the top of conical patch, and a factor of two for two-sided mass loss. For a half-cone angle of θ the area $A = z^2 \int_0^{2\pi} \int_0^{\theta} \sin(\theta')d\theta' d\phi$.

$$\frac{dP_c}{dt} = M_c \frac{dv}{dt} = F_{\rm ram} + F_{\rm rad} - F_{\rm grav}, \tag{1}$$

where M_c is the mass of the cloud and v is its velocity in the z-direction. $F_{\rm ram}$ represents the force exerted by the hot wind via ram pressure in g cm s^{-2}. $F_{\rm rad}$ is the force due to radiation on dust grains and $F_{\rm grav}$ is the gravitational force.

We first discuss the role of ram pressure on the motion of cold blobs of gas dragged in it, following the model of Strel'nitskii & Sunyaev (1973). In this scenario, the hot gas observed in X-rays and which is thought to provide the ram pressure has temperatures in the range 0.5–1 keV (Heckman 2002; Martin 2005), which correspond to the isothermal sound speed $c_s \sim 300$–400 km s^{-1}. Current X-ray instruments cannot detect the speed of this hot and tenuous material and hence the kinemetics of this hot phase is poorly constrained. If we assume it as an adiabatic wind passing through a sonic point, then $v_h^2 \sim \alpha c_s^2$, where $\alpha = 2.5$–5 (Efstathiou 2000), which gives $v_h \sim 1.2$–$2.2\,c_s$. In this paper, we take $v_h \sim 800$ km s^{-1}, which corresponds to $v_h \sim 2c_s$ and $T_X \sim 1$ keV.

Consider then the hot gas flow (with density ρ_h and velocity v_h), emerging through a cone. Mass loss in a hot wind is given by the following expression (see Figure 1):

$$\dot{M}_h = 2\rho_h v_h z^2 \int_0^{2\pi} \int_0^{\theta} \sin(\theta')d\theta' d\phi. \tag{2}$$

Observations indicate conical angles for hot wind in the range $2\theta \sim 10^\circ$–100° (Veilleux et al. 2005; Lehnert & Heckman 1996). We consider a mass-loss rate of $\dot{M}_h \approx (\pi/2) z^2 \rho_h v_h$, which roughly corresponds to half-cone angle $\theta \sim 30^\circ$. The momentum injection rate is $\dot{p}_h = \dot{M}_h v_h$, so we can write

$$\rho_h v_h^2 = \frac{\dot{p}_h}{\pi z^2/2}. \tag{3}$$

The force exerted by the ram pressure on a cold cloud of mass M_c and cross-section A_c is given by

$$\begin{aligned} F_{\rm ram} &= \frac{1}{2} C_D A_c \rho_h (v_h - v)^2\, \mathcal{H}(v_h - v) \\ &= \frac{C_D A_c}{2} \rho_h v_h^2 \left(1 - \frac{v}{v_h}\right)^2 \mathcal{H}(v_h - v). \end{aligned} \tag{4}$$

Here $\mathcal{H}(v_h - v)$ is the step function whose value is 1 for $v < v_h$ and 0 otherwise. $C_D \sim 0.5$ is the drag coefficient. For the cloud, one can write $M_c/A_c = \mu m_p N_{\rm H}$, where $N_{\rm H}$ is the column density and μ is the mean molecular weight. Also the momentum injection rate $\dot{p}_h$ is $\sim[5 \times 10^{33}\,({\rm SFR}/1\,M_\odot\,{\rm yr}^{-1})]$ dyne in a starburst (Leitherer et al. 1999). Using these and substituting Equation (3) into Equation (4) we get

$$\frac{F_{\rm ram}}{M_c} = \frac{\left[5 \times 10^{33} \left(\frac{\rm SFR}{1\,M_\odot\,{\rm yr}^{-1}}\right)\right] {\rm dyne}}{4\,N_{\rm H}\,\mu m_p\,(\pi z^2/2)} \left(1 - \frac{v}{v_h}\right)^2 \mathcal{H}(v_h - v). \tag{5}$$

Next we consider the forces due to a galactic disk. We will use f for force per unit mass ($f = F/M_c$). In cylindrical geometry, the force of gravitation $f_{g,d}(z)$, and that due to radiation $f_{r,d}(z)$, along the pole of a disk of radius r_d, with constant surface density (Σ) and surface brightness (I) are given by

$$\begin{aligned} f_{g,d} &= 2\pi G\Sigma \int^{r_d} \frac{z r dr}{(r^2 + z^2)^{3/2}}, \\ f_{r,d} &= \frac{2\pi\kappa I}{c} \int^{r_d} \frac{z^2 r dr}{(r^2 + z^2)^2}, \end{aligned} \tag{6}$$

where κ is the average opacity of a dust and gas mixture. The ratio of these forces, the Eddington ratio, increases with the height z, beginning with a value of $\Gamma_0 = \kappa I/2cG\Sigma$ at the disk center at $z = 0$. Since $I/\Sigma \propto L/M_d$, where M_d is the disk mass, we can express Γ_0 in terms of the SFR by calculating the luminosity L of a galaxy in any desired band for a certain SFR using the Starburst99 code (Vásquez & Leitherer 2005). The luminosity in this case is proportional to SFR, therefore if L_1 is the luminosity at 1 Gyr for an SFR of 1 $M_\odot$ yr^{-1} then we can write Γ_0 as

$$\Gamma_0 = \frac{\kappa}{2cG} \frac{L_1 \times \frac{\rm SFR}{1\,M_\odot\,{\rm yr}^{-1}}}{M_d}. \tag{7}$$

We use the mean opacity for gas mixed with dust $\sim$200 cm^2 g^{-1} corresponding to a color temperature $\sim$9000 K in the U band (Figure 1(b), Draine 2011).

To determine the gravitational force, we assume a spherical mass distribution in the bulge and halo. For the bulge, we assume a total mass of $M_b \sim 0.1 M_d$ inside a radius $r_b \sim 0.1 r_d$ for simplicity. For the halo, we consider a Navarro–Frenk–White (NFW) profile, with total mass $M_{\rm vir}$ (Navarro et al. 1997). We fix $M_{\rm vir}$ for a given disk mass (M_d), by the ratio $M_{\rm vir}/M_d \sim 20$, as determined by Mo et al. (1998, referred to as MMW98 hereafter). We evaluate the disk exponential scale length (r_d) using the prescription of MMW98 and use it as the size of galactic disk. Gravitational potential of NFW halo is

$$\Phi_{\rm NFW} = -\frac{G M_{\rm vir}}{\ln(1+c) - c/(1+c)} \left[\frac{\ln\left(1 + \frac{R}{R_s}\right)}{R}\right], \tag{8}$$

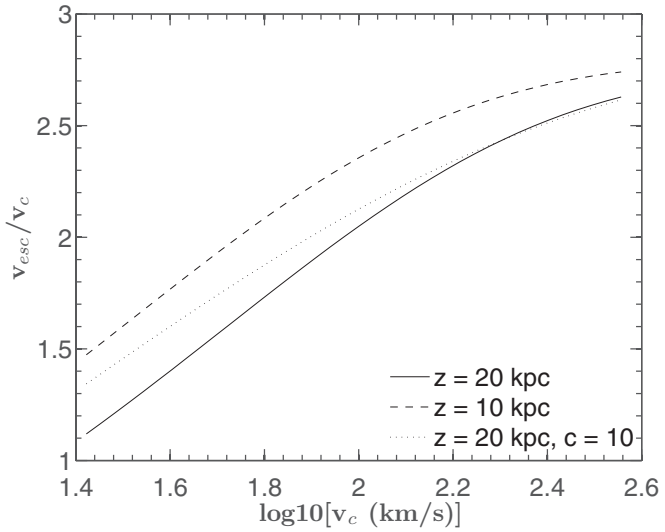

Figure 2. Ratio of NFW escape speed to the circular speed vs. the circular speed, at two different vertical distances, 10 kpc (dashed line) and 20 kpc (solid line). The dotted line is for a fixed value of halo concentration parameter $c = 10$.

where $R = \sqrt{r^2 + z^2}$, $c = R_{200}/R_s$ is the concentration parameter, R_s is the NFW scale length, and R_{200} is the radius within which the mean overdensity is 200. This potential implies a gravitational force along z which is given by

$$f_{\rm halo,z} = \left| -\frac{\partial \Phi_{\rm NFW}}{\partial z} \right|_{r=0} = \frac{GM_{\rm vir}}{z^2} \left[\frac{\ln\left(1+\frac{z}{R_s}\right) - z/(z+R_s)}{\ln(1+c) - c/(1+c)} \right]. \quad (9)$$

The rotation speed implied by the NFW profile peaks at a radius $R \sim 2R_s$, given by,

$$v_c^2 = v_{200}^2 \, \frac{c}{2} \, \frac{\ln(3) - 2/3}{\ln(1+c) - c/(1+c)}, \quad (10)$$

where v_{200} is the rotation speed at R_{200}. We choose this value of the maximum rotation speed to represent the v_c of the disk galaxy, since Figure 2 of MMW98 shows that the value of v_c from the flat part of the total rotation curve does not differ much from the peak of the rotation curve from halo only. The escape speed in an NFW halo is given by

$$v_{\rm esc}^2 = v_c^2 \left[\frac{4}{\ln(3) - \frac{2}{3}} \left(\frac{R_{200}}{R} \ln\left(1 + \frac{cR}{R_{200}}\right) - \frac{c}{1+c} \right) \right]. \quad (11)$$

Figure 2 shows the escape speed along the z-axis for different galaxies. The dashed and solid lines show the escape speed at 10 and 20 kpc from the disk plane, for galaxies with different circular speed. We have used the relation between the halo concentration parameter c and galactic mass as given by Maccio et al. (2007). We find that for low-mass galaxies with $v_c \leqslant 100$, the escape velocity $v_{\rm esc} \lesssim 2v_c$, and that for higher mass galaxies, the escape speed ranges between 2 and 3 v_c. We can therefore conclude that for escaping winds, the ratio of wind speed to circular speed should be in the range of 2–3.

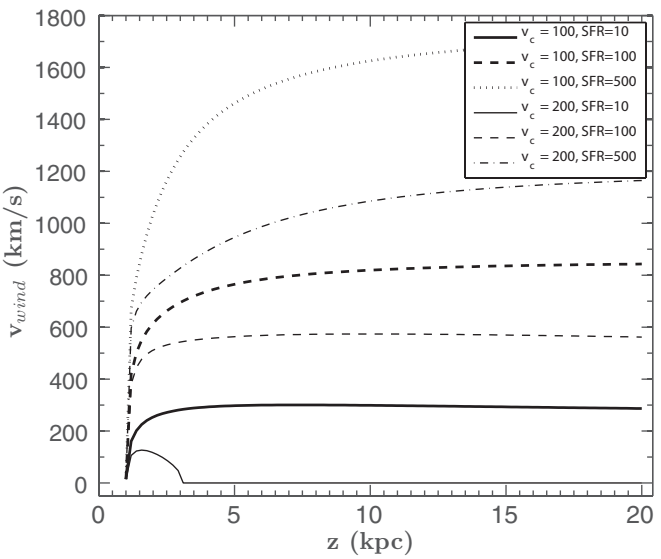

Figure 3. Variation of wind speed with vertical distance (z) for galaxies of different circular speeds. The thick solid, dashed, and dotted lines refer to $v_c = 100$ km s^{-1}, and for SFR of 10, 100, 500 $M_\odot$ yr^{-1}, respectively. The thin solid, dashed, and dot-dashed lines refer to $v_c = 200$ km s^{-1}, for the same values of SFR, respectively.

One can finally rewrite Equation (1) for evaluating the velocity of clouds as a function of z,

$$v\frac{dv}{dz} = \frac{\left[5 \times 10^{33} \left(\frac{\rm SFR}{1\, M_\odot\, {\rm yr}^{-1}}\right)\right] {\rm dyne}}{4N_{\rm H}\, \mu m_p\, (\pi z^2/2)} \left(1 - \frac{v}{v_h}\right)^2 \mathcal{H}(v_h - v) + 2\pi G\Sigma\Gamma_0 \left(\frac{r_d^2}{z^2 + r_d^2}\right) - 2\pi G\Sigma \left(1 - \frac{z}{\left(z^2 + r_d^2\right)^{1/2}}\right) - \frac{GM_b}{z^2} - \frac{GM_{\rm vir}}{z^2} \left(\frac{\ln\left(1+\frac{z}{R_s}\right) - \frac{z}{z+R_s}}{\ln(1+c) - \frac{c}{1+c}} \right), \quad (12)$$

where Γ_0 is given by Equation (7). We use $\mu = 1.4$ and $N_{\rm H} \sim 10^{21}$ cm^{-2} (Martin 2005; Heckman et al. 2000). Here the first term on the right-hand side denotes ram pressure, the second term the radiation pressure, and the last three terms represent the gravity of the disk, bulge, and NFW halo, respectively. This equation is nonlinear due to the presence of v in the ram pressure term and should be solved numerically, although previous authors have approximated it assuming $v \ll v_h$. The form of the ram pressure term suggests that ram pressure would not be effective once the velocity becomes greater than the velocity of the hot component. Hence, the ram pressure is likely to be effective for low-mass galaxies.

3. RESULTS

We solve the wind equation (Equation (12)) numerically. Figure 3 shows the wind speed as a function of z for different values of SFR for two galaxies, with $v_c = 100$ km s^{-1} and $v_c = 200$ km s^{-1}. Instead of rising continuously, the wind speed saturates after traveling a distance of $\geqslant$10 kpc, with a terminal speed that is lower for higher mass galaxies. The thick solid line roughly corresponds to M82, and the wind speed $\sim$300 km s^{-1} is consistent with observations (Heckman et al. 2000; Schwartz & Martin 2004).

We then use the wind speed at $z = 20$ kpc and show the variation of v_w/v_c with circular speed v_c and SFR in the left

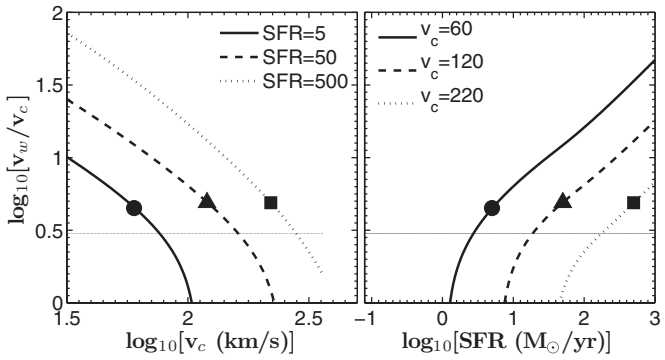

Figure 4. Ratio of wind velocity at 20 kiloparsec and the galactic rotation speed plotted with v_c for three different SFR in the left panel and with SFR for three different v_c in the right panel. Three representative cases are shown with solid circle (dwarf starbursts), solid triangle (LIGs), and solid square (ULIGs). The thin horizontal line corresponds to $v_w = 3v_c$.

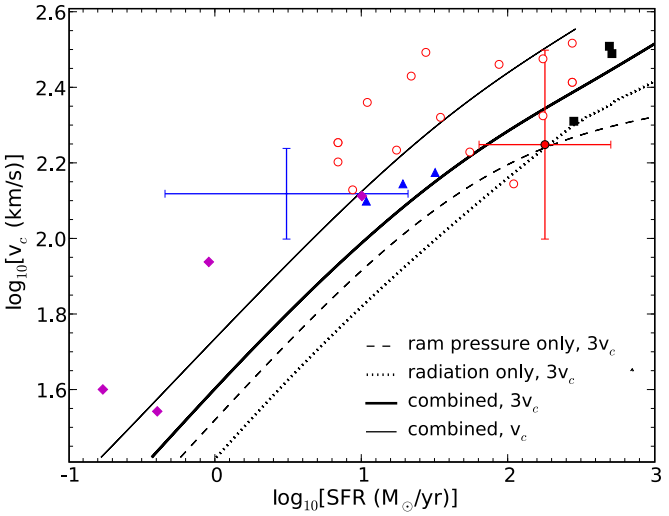

Figure 5. Contours of $v_{w,20\,\mathrm{kpc}}$ in units of v_c for winds driven by only ram pressure, only radiation pressure, and a combination of the two. The wind velocity increases as one moves from top left corner to bottom right corner. Also plotted are the data points with different symbols: hollow circles (Heckman et al. 2000), squares (Martin 2005; Genzel et al. 2001), triangles (Weiner et al. 2009), diamonds (Schwartz & Martin 2004), big red cross with circle at its center (Rupke et al. 2005), and big blue cross (Tumlinson et al. 2011) without two outliers in SFR.

(A color version of this figure is available in the online journal.)

and right panels of Figure 4, respectively. We find that, for a constant SFR, v_w/v_c decreases with v_c, as gravity increases with v_c. We also show three representative cases in this plot of dwarf starbursts (solid circle: $v_c \sim 60$ km s^{-1}, SFR $\sim 5\,M_\odot$ yr^{-1}), LIGs (solid triangle: $v_c \sim 120$ km s^{-1}, SFR $\sim 50\,M_\odot$ yr^{-1}), ULIGs (solid square: $v_c \sim 220$ km s^{-1}, SFR $\sim 500\,M_\odot$ yr^{-1}). The values of v_w/v_c lie close to $\sim$3 which is shown by the thin horizontal line. The near constancy of v_w/v_c for the three representative points recovers the observed scaling of v_w with v_c. Taking into account the variation of v_w/v_c with v_c and SFR we find that the results can be approximated by the following fit:

$$\frac{v_w}{v_c} \sim 10^{0.7}\left[\frac{\mathrm{SFR}}{50\,\mathrm{M_\odot\,yr^{-1}}}\right]^{0.4}\left[\frac{v_c}{120\,\mathrm{km\,s^{-1}}}\right]^{-1.25}. \quad (13)$$

Next we solve the wind equation for a grid of SFR and galaxy circular speed values, for the cases of ram pressure and radiation pressure alone, and then for the combination of the two. In Figure 5, the wind velocity is zero in the top left corner for high-mass and low SFR galaxies. Wind velocity increases as one moves diagonally, from the top left to the bottom right corner. We show two contours for $v_w = 3v_c$ with thin solid lines for ram and radiation pressure alone. For the case of combined ram and radiation pressure driving, we show two contours, for $v_w = v_c$ and $3v_c$ (upper and lower thick lines). We also show the data for outflows from a number of observations (see the caption for details).

In the case of only radiation pressure, the wind speed is found to be roughly proportional to SFR, which can be understood from the fact that $\Gamma_0 \propto$ SFR. The case for only ram pressure appears to explain the wind in low-mass galaxies. However, from the $v_w = 3v_c$ contour it is clear that ram pressure cannot drive the cold clouds out of the galaxies with rotation speeds $\gtrsim$200 km s^{-1}, as we have seen in the previous section that for escaping winds one needs $v_w \sim 3v_c$. This points to the existence of a critical rotation speed above which the physical mechanism of outflow changes. Therefore, outflows from galaxies with $v_c \leqslant 200$ km s^{-1} and SFR $\leqslant 100\,M_\odot$ yr^{-1} are dominated by ram pressure and those from the more massive galaxies with larger SFR are influenced more by radiation pressure.

4. DISCUSSIONS

The most important result of our calculation is that galactic outflows require both ram and radiation pressure, especially for high-mass and high SFR cases. Our calculation has a number of ingredients from stellar physics and disk and halo parameters, and apart from the value of the hot wind speed v_h, there is no free parameter in this calculation. It is therefore interesting to note that our theoretical results are consistent with most data of outflows when studied in the parameter space of v_c and SFR. It is also interesting that a recent simulation with ram and radiation pressure-driven outflows has concluded that these two processes are important in different mass regimes, although it is not clear where the dividing line between the two regimes lies (Hopkins et al. 2012; van de Voort & Schaye 2011). Outflowing clouds from galaxies on the left of the contours in Figure 5 are unlikely to escape into the IGM and likely get trapped in the circumgalactic region as observed by Tumlinson et al. (2011; data shown by blue cross) or fall back (Oppenheimer & Davé 2008).

Although strictly speaking our calculation refers to cold clouds being driven out along the pole of the disk galaxies, and we cannot infer the mass-loss rate without doing a two-dimensional calculation, but we can speculate on the scaling of the mass-loss rate with galactic mass by making some simple assumption. Let us assume that the dynamics of cold clouds beyond the polar regions are similar to that along the pole. Assuming a one-dimensional mass flow, the mass-loss rate from the disk is approximately $\dot{M}_w \propto v_w[\Sigma_g \pi r_d^2]$, where Σ_g is the gas column density and r_d is the scale length of the disk. We note that in the prescription of MMW98 one has $v_c \propto r_d$. We therefore have $\dot{M}_w \propto v_c^{2-0.25}\dot{M}_*^{0.4}\Sigma_g$, where we have used Equation (13), after multiplying both sides by v_c. The ratio of the mass outflow rate to the SFR is therefore $\dot{M}_w/\dot{M}_* \propto v_c^{1.75}\Sigma_g \dot{M}_*^{-1.4}$. Using Kennicutt's law of star formation, which gives $\dot{M}_* \propto \Sigma_g^{1.4} r_d^2 \propto \Sigma_g^{1.4} v_c^2$, we have finally, $\dot{M}_w/\dot{M}_* \propto v_c^{-1.05}\Sigma_g^{-0.96}$. We can therefore conclude that roughly

$$\frac{\dot{M}_w}{\dot{M}_*} \propto v_c^{-1}\Sigma_g^{-1}. \quad (14)$$

Interestingly, similar power-law dependence has also been found in simulations (Hopkins et al. 2012).

We note that our results assumed a value of $v_h \sim 800$ km s^{-1} and a column density of cold clouds of $\sim 10^{21}$ cm^{-2}. If we assume a larger value of v_h ($\sim$1000 km s^{-1}), then the contour for only ram pressure will be able to explain the winds in ULIGs with large SFR and high mass. A similar result will follow from larger values of κ for the radiation pressure case.

It is interesting to note that the contour for only radiation pressure can explain the ULIG region of Figure 5 (top right corner). Extending to larger SFR, our results indicate that radiation pressure will also be important for hyperluminous infrared galaxies (Rowan-Robinson 2000). Lastly, although it may appear that the role of radiation pressure in galaxies other than ULIGs is less dominant than ram pressure as far as energetics is concerned, radiation pressure may still play an important role in lifting the clouds to a large height before it is embedded in the hot wind to help it survive long (Nath & Silk 2009; Murray et al. 2011).

5. SUMMARY

We have studied the outflows from disk galaxies driven by ram and radiation pressure and compared the theoretical results with data in the parameter space of galaxy circular speed and SFR. We found that the driving mechanism of escaping wind is different in low-mass and high-mass galaxies, with radiation pressure being important for high-mass galaxies with high SFR. Our results are also consistent with recently observed circum-galactic gas.

We thank Mitchell Begelman, Bruce Draine, Tim Heckman, Yuri Shchekinov, and an anonymous referee for valuable comments.

REFERENCES

Chevalier, R. A., & Clegg, A. W. 1985, Nature, 317, 44
Dekel, A., & Silk, J. 1986, ApJ, 303, 39
Draine, B. T. 2011, ApJ, 732, 100
Efstathiou, G. 2000, MNRAS, 317, 697
Ferrara, A., Pettini, M., & Shchekinov, Y. 2000, MNRAS, 319, 539
Genzel, R., Tacconi, L. J., Rigopoulou, D., Lutz, D., & Tecza, M. 2001, ApJ, 563, 527
Heckman, T. M. 2002, in ASP Conf. Ser. 254, Extragalactic Gas at Low Redshift, ed. L. S. Mulchaey & J. Stocke (San Francisco, CA: ASP), 292
Heckman, T. M., Lehnert, M. D., Strickland, D. K., & Armus, L. 2000, ApJS, 129, 493
Hopkins, P. F., Quataert, E., & Murray, N. 2012, MNRAS, in press
Larson, R. B. 1974, MNRAS, 169, 229
Lehnert, M. D., & Heckman, T. M. 1996, ApJ, 462, 651
Leitherer, C., Schaerer, D., Goldader, J. D., et al. 1999, ApJS, 123, 3
Macció, A. V., Dutton, A. A., van den Bosch, F. C., et al. 2007, MNRAS, 378, 55
Madau, P., Ferrara, A., & Rees, M. J. 2001, ApJ, 555, 92
Martin, C. L. 1999, ApJ, 506, 222
Martin, C. L. 2005, ApJ, 621, 227
Mo, H. J., Mao, S., & White, S. D. M. 1998, MNRAS, 295, 319 (MMW98)
Murray, N., Meńard, B., & Thompson, T. A. 2011, ApJ, 735, 66
Murray, N., Quataert, Q., & Thompson, T. A. 2005, ApJ, 618, 569
Nath, B. B., & Silk, J. 2009, MNRAS, 396, L90
Nath, B. B., & Trentham, N. 1997, MNRAS, 291, 505
Navarro, J. F., Frenk, C. S., & White, S. D. M. 1997, ApJ, 490, 493
Oppenheimer, B. D., & Davé, R. 2008, MNRAS, 387, 5770
Rowan-Robinson, M. 2000, MNRAS, 316, 885
Rupke, D. S., Veilleux, S., & Sanders, D. B. 2005, ApJS, 160, 115
Saito, M. 1979, PASJ, 31, 193
Schwartz, C. M., & Martin, C. L. 2004, ApJ, 610, 201
Sharma, M., Nath, B. B., & Shchekinov, Y. 2011, ApJ, 736, L27
Strel'nitskii, V. S., & Sunyaev, R. A. 1973, SvA, 16, 579
Strickland, D. K., & Stevens, I. R. 2000, MNRAS, 314, 511
Suchkov, A. A., Balsara, D. S., Heckman, T. M., & Leitherer, C. 1994, ApJ, 430, 511
Tumlinson, J., Thom, C., Werk, J. K., et al. 2011, Science, 334, 948
van de Voort, F., & Schaye, J. 2011, arXiv:1111.5039
Vásquez, G. A., & Leitherer, C. 2005, ApJ, 621, 695
Veilleux, S., Cecil, G., & Bland-Hawthorn, J. 2005, ARA&A, 43, 769
Weiner, B. J., Coil, A. L., Prochaska, J. X., et al. 2009, ApJ, 692, 187